Probabilistic Analysis for Large Strain Radial Consolidation of Soft Soils considering Creep

by
Ding-Bao Song, Research Assistant Professor
College of Civil and Transportation Engineering, Shenzhen University, Shenzhen, China.
Department of Civil and Environmental Engineering, The Hong Kong Polytechnic University,
Hung Hom, Kowloon, Hong Kong.
Email: dingbao.song@polyu.edu.hk or dingbao_song@126.com

Zhen-Yu Yin, Professor (Corresponding author)
Department of Civil and Environmental Engineering, The Hong Kong Polytechnic University,
Hung Hom, Kowloon, Hong Kong.
Email: zhenyu.yin@polyu.edu.hk

Jian-Hua Yin, Chair Professor
College of Civil and Transportation Engineering, Shenzhen University, Shenzhen, China.
Department of Civil and Environmental Engineering, The Hong Kong Polytechnic University,
Hung Hom, Kowloon, Hong Kong.
Email: jian-hua.yin@polyu.edu.hk

Manuscript submitted to *Canadian Geotechnical Journal*

6 August 2025

Abstract: Effective design of prefabricated vertical drains (PVDs) requires accurate prediction of soil consolidation behavior incorporating creep and spatial variability in soil properties. This study develops a probabilistic analysis framework that integrates random field theory, the piecewise-linear method and Monte Carlo simulation to evaluate the long-term consolidation of soft soils with PVDs. The framework accounts for spatial variability in soil parameters, creep strain, large-strain effects, hydraulic conductivity anisotropy, soil smear, and time-dependent loading. Three routinely measured soil parameters, including plasticity index, liquid limit, and void ratio, are treated as random variables. The proposed method is validated through comparison with field measurements from a preloaded embankment site along the Sydney-Newcastle Freeway extension equipped with PVDs. Results show that the field data align closely with the high-probability density predictions from the probabilistic analysis. Sensitivity analysis indicates that increasing the coefficient of variation leads to an almost linear widening of the estimated range, while autocorrelation distances and cross-correlation coefficients exert a relatively minor influence on consolidation behavior. These findings highlight the importance of accurately estimating the coefficient of variation in a cost-effective manner during field investigations and statistical analysis.

Keywords: Soft soils; Large-strain consolidation; Creep; Prefabricated vertical drains; Probabilistic analysis

Introduction

Subsurface conditions at many construction sites are characterized by thick layers of compressible soft soils. Similarly, dredged soil slurries are frequently used in land reclamation projects due to the scarcity and increasing cost of high-quality granular fill materials (Yozzo et al. 2004; Yin et al. 2024). To address these challenges, vertical drains combined with preloading, using surcharge, vacuum, or both, are employed to improve the stiffness and strength of soft soils. Although early projects utilized sand drains as vertical drainage channels, they have largely been replaced by prefabricated vertical drains (PVDs), which are band-shaped, cost-efficient, and easier to install. The installation of closely spaced PVDs shortens the maximum drainage path and redirects the primary fluid flow direction from the vertical to the horizontal direction, where hydraulic conductivity is typically greater. This significantly accelerates the consolidation process in soft soil layers.

PVDs are now widely used to improve soft soils in various infrastructure projects, including embankment (Chai et al. 2001; Lo et al. 2008; Baral et al. 2021), disposal sites (Nozue et al. 2007), storage facilities (Chu et al. 2000), reclaimed lands (Zhu et al. 2018), airport runways (Tang and Shang 2000; Bergado et al. 2002), and ports (Indraratna et al. 2019). Radial consolidation models play a central role in PVD design, allowing engineers to optimize drain layouts and predict pore pressure dissipation and settlement over time. Spatial variability in the physical and mechanical parameters of soils arises from natural processes such as sedimentation, historical loading, and chemical or physical weathering (Phoon and Kulhawy 1999; Nishimura et al. 2002). However, laboratory or in situ measurements at discrete locations often fail to adequately capture this variability. Incorporating spatial variability into consolidation analysis is essential for accurately modeling soil behavior (Huang et al. 2007; Bong et al. 2014; Spross and Larsson 2021). Despite this, most existing studies on spatial variability in coupled consolidation problems are limited to small-strain theory and do not fully incorporate random field applications (Huang et al. 2010; Shi and Wang 2023).

Finite strain consolidation theory, which accounts for changes in soil thickness under loading, offers significant advantages in analyzing soft soils with vertical drains, especially in layered ultra-soft conditions. In the context of deterministic analysis, researchers have made valuable contributions to modeling consolidation under finite strain, incorporating factors such as non-Darcian radial flow (Indraratna et al. 2017), creep strains (Song et al. 2024), general constitutive relationships (Pu et al. 2020), well resistance (Nguyen et al. 2020), cyclic loading (Ni and Geng 2022) and various solution techniques, such finite differences (Hu et al. 2014; Li et al. 2024), finite element (Geng and Yu 2017), and piecewise-linear (Fox et al. 2003; Song et al. 2024). Among these, the piecewise-linear numerical model RCS1, designed for single-layer saturated soils, accounts for vertical drain, soil self-weight, hydraulic conductivity anisotropy, radial and vertical flows, soil smear effects, and evolving material properties during consolidation. The piecewise-linear approach is particularly effective in handing spatial nonlinearity, material heterogeneity, and complex initial or boundary conditions. These advancements provide a robust framework for modeling large-strain radial consolidation.

This study presents a probabilistic analysis framework for modeling the long-term finite strain consolidation of soft soils with prefabricated vertical drains (PVDs), utilizing a piecewise-linear approach and an elastic visco-plastic constitutive model. The framework incorporates critical factors such as the spatial variability of soil parameters, creep behavior, large-strain effects, hydraulic conductivity anisotropy, radial and vertical flows, soil smear, time-dependent loading, and variations in hydraulic conductivity and compressibility throughout the consolidation process. Three on-site measurable soil parameters, including plasticity index, liquid limit, and void ratio, are treated as random variables. Spatial variability in constitutive parameters is quantified using empirical relationships linking these measurable inputs to the parameters required for analysis. The development of this framework is outlined, followed by validation using a field case study of a preloaded site on the Sydney-Newcastle Freeway, involving thick layers of soft clay and large strains. The study also evaluates the influence of the coefficient of variation, vertical and lateral autocorrelation distances, and cross-correlation coefficients on the probabilistic analysis of radial consolidation in soft clay.

Consolidation Model

Geometry

A saturated, homogeneous soil layer with an initial height H_o is idealized as a two-phase material comprising incompressible pore water and solid particles. The term "homogeneous" refers to the constitutive relationships of the soil layer rather than its initial conditions, such as void ratio of effective stress distributions. For consolidation analysis involving a single drain, an axisymmetric unit cell with an effective influence radius r_e is typically adopted, reflecting the regular grid arrangement of vertical drains. Fig. 1 illustrates the initial geometry of an axisymmetric soil column with a height H_o and radius r_e before load application (t = 0). Drains may fully or partially penetrate the soil layer, with penetration length $L_d \leq H_o$. The drain radius r_w is calculated as $r_w = (w_d + t_d)/\pi$, where w_d and t_d are the width and thickness of the PVD band. The surrounding smear zone is modeled with an equivalent radius r_s.

Anisotropic hydraulic conductivity is incorporated in the analysis by assigning k_v for the vertical direction and k_r (= $r_k k_v$) for the radial direction, where r_k is assumed throughout the consolidation process and is consistent with the findings by Leroueil et al. (1990). In the smear zone, hydraulic conductivity is also modeled as anisotropic, with k_{sv} in the vertical direction and k_{sr} (= $r_k k_{sv} = k_r/\eta$) in the radial direction, where η is the hydraulic conductivity ratio of the smear zone. A constant η, typically ranging from 2 to 6 as recommended, is adopted in the RCS-EVP model. The soil column is discretized into R_j elements vertically and R_i elements radially, with the first Rs radial elements defining the smear zone. This creates a mesh of $R_j \times R_i$ axisymmetric ring elements. The vertical coordinate z is positive upward from the bottom of the soil layer, while the radial coordinate r is positive outward from the drain center. Element coordinates i and j follow a similar convention. Each ring element has an initial rectangular cross-section with width d_i, height $L_o = H_o/R_j$, and volume $V_{oi} = 2\pi r_i d_i L_o$, centered at an initial elevation z_{oj}, where $d_i = (r_s\text{-}r_w)/R_s$ for the smear zone, $d_i = (r_e\text{-}r_s)/(R_i\text{-}R_s)$ for the undisturbed soil. Boundary conditions can be specified as undrained, freely drained, or vacuum pressure-controlled at the top and bottom of the soil column. The outer lateral boundary ($r = r_e$) is typically assumed impermeable due to the symmetry of adjacent unit cells. Flow resistance in the drain (i.e., well resistance) is neglected in the RCS-EVP model.

A time-dependent vertical surcharge load, Δq^t, is applied to the top boundary of the soil layer, moving vertically in tandem with the upper boundary throughout the consolidation process. The boundary condition at the drain can be specified as impermeable, freely drained, or vacuum pressure controlled. In vacuum preloading with a permeable sand drainage blanket and an airtight membrane covering the upper soil boundary, vacuum pressure is applied simultaneously at the top boundary and within the drain. Alternatively, in the membrane-less vacuum preloading method, where the vacuum pump system is directly connected to PVDs, the sand blanket is unnecessary. This scenario can be modeled by specifying the drain boundary condition as vacuum drainage. Excess pore pressure, generated by applied surcharge or vacuum pressure boundary conditions, drives fluid flow from the interior of the soil column to all drainage boundaries. Soil deformation occurs due to fluid outflow from each ring element and is assumed to be purely vertical, transforming the element's cross-section into a trapezoidal shape with constant lateral spacing d_i, as shown in Fig. 1(b).

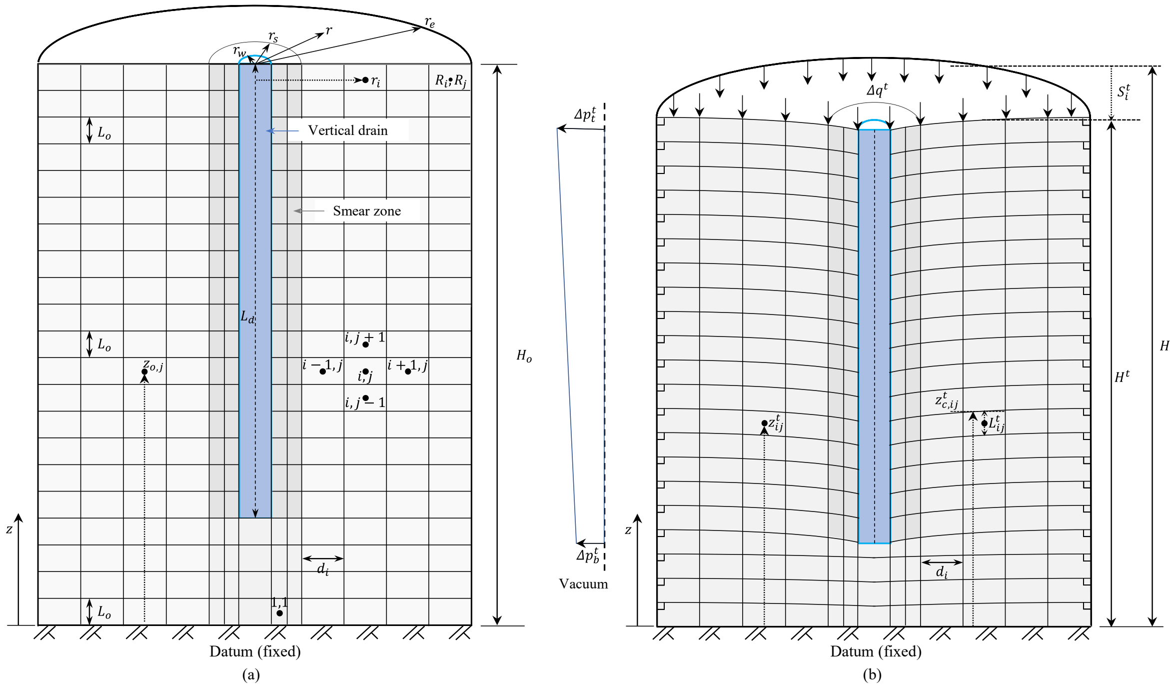

Fig. 1. Geometry for RCS-EVP: (a) initial configuration ($t = 0$), and (b) after consolidation for time t_1 ($t_1 > 0$)

During the consolidation process ($t > 0$), the average height L_{ij}^t and node elevation z_{ij}^t for ring element ij are calculated as

(1) $$L_{ij}^t = \frac{z_{c,ij}^t + z_{c,i-1,j}^t - z_{c,i,j-1}^t - z_{c,i-1,j-1}^t}{2}$$

(2) $$z_{ij}^t = \frac{z_{c,i-1,j-1}^t + z_{c,i-1,j}^t + z_{c,i,j-1}^t + z_{c,ij}^t}{4}$$

where $z_{c,m,ij}^t$ = elevation of the upper outer corner of ring element, as illustrated in Fig. 1(b). Corner elevations of element are calculated as

(3) $$z_{c,ij}^t = z_{c,i-1,j}^t + z_{c,i,j-1}^t - z_{c,i-1,j-1}^t + \frac{3d_i\left[V_{ij}^t - \pi\left(z_{c,i-1,j}^t - z_{c,i-1,j-1}^t\right)\left(r_{ou}^2 - r_{in}^2\right)\right]}{\pi\left(r_{in}^3 - 3r_{in}r_{ou}^2 + 2r_{ou}^3\right)}$$

where V_{ij}^t = volume of element ij at time t, $r_{in} = r_i - \left(d_i/2\right)$ and $r_{ou} = r_i + \left(d_i/2\right)$ are the internal and outer radial coordinates of element i. Cross-sections of the outmost ring elements, i.e., $i = R_i$, are assumed to remain rectangular during the entire consolidation process to ensure that all of the corner elevations can be determined from the volume values.

Constitutive Relationships

The elastic visco-plastic (EVP) constitutive model, developed by Yin and Graham (1989, 1994), is incorporated into the RCS-EVP framework. Fig. 2(a) illustrates the effective stress-void ratio relationship as a function of time, based on the EVP model. The change in void ratio *de* over a time increment *dt* is calculated using Eq. (4). Conversely, if *de* and *dt* are known, the corresponding increment in effective stress $d\sigma'$ can be determined using Eq. (5).

(4)
$$de = \frac{\kappa}{\sigma'} d\sigma' + \frac{\psi}{t_o} \exp\left(\frac{e - e_o^r}{\psi}\right)\left(\frac{\sigma'}{\sigma'_{ro}}\right)^{\lambda/\psi} dt$$

(5)
$$d\sigma' = \left(de - \frac{\psi}{t_o} \exp\left(\frac{e - e_o^r}{\psi}\right)\left(\frac{\sigma'}{\sigma'_{ro}}\right)^{\lambda/\psi} dt\right) \times \frac{\sigma'}{\kappa}$$

where σ' = vertical effective stress; κ, λ and ψ = slope of instant time line dependent on $\ln\left(\sigma'/\sigma'_i\right)$, the slope of a reference time line related to $\ln\left(\sigma'/\sigma'_{ro}\right)$, and the slope of a creep line associated with $\ln\left[\left(t_o + t_e\right)/t_o\right]$, respectively, where σ'_i = unit-reference effective stress for an instant time line and t_e = equivalent time; σ'_{ro} = stress in the reference time line and is similar to the pre-consolidation pressure; and t_o = a constant soil parameter. Details of the extended EVP model derivation are provided by Song et al. (2023a).

The hydraulic conductivity relationship implemented in RCS-EVP (Fig. 2b) is defined using R_n (≥ 2) pairs of vertical hydraulic conductivity $\bar{k}_v$ and void ratio $\bar{e}$. This flexible approach allows any desired form of the hydraulic conductivity relationship to be approximated by selecting an appropriate number of discrete data pairs. Once the void ratio of element *ij* at time *t*, e_{ij}^t, is determined, the corresponding vertical hydraulic conductivity ($k^t_{v,ij}$) can be calculated by interpolating between the adjacent defined data pairs.

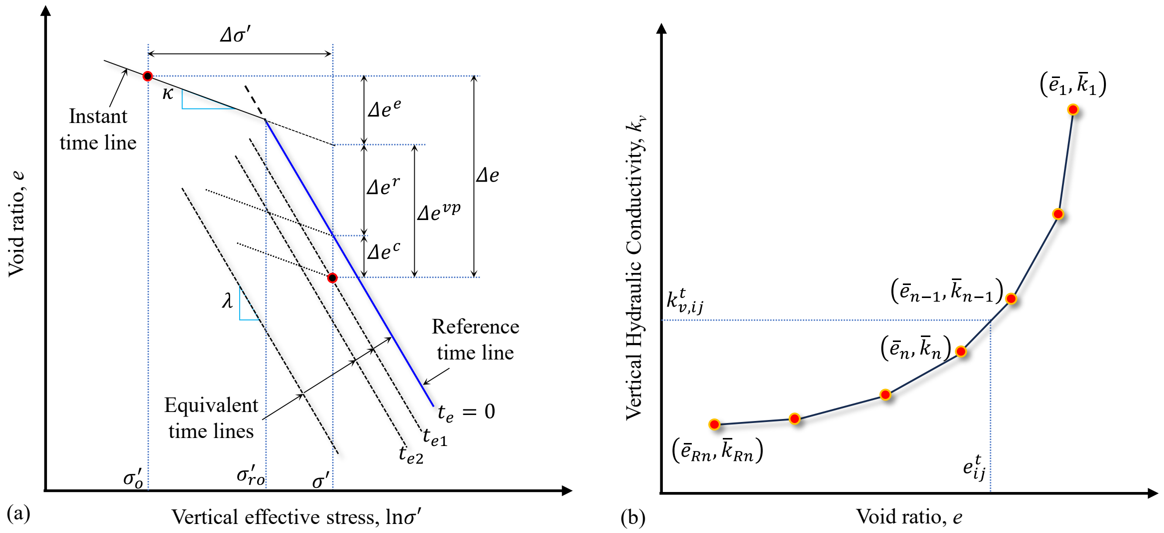

Fig. 2. Soil constitutive relationships: (a) elastic visco-plastic compressibility and (b) hydraulic conductivity

Stress, Flow and Settlement

The vertical total stress at node ij at time t, σ^t_{ij}, is calculated by considering the self-weight of the overlying soil layer and the overburden effective stress, as expressed by

$$\sigma^t_{ij} = \left(h_t - \frac{z^t_{c,i-1,R_j} + z^t_{c,i,R_j}}{2} \right) \gamma_w + \sigma'_{o,ij} + \Delta q^t + \frac{V^t_{ij}\gamma^t_{ij}}{4\pi r_i d_i} + \sum_{b=j+1}^{R_j} \frac{V^t_{ib}\gamma^t_{ib}}{2\pi r_i d_i} \tag{6}$$

where $\gamma^t_{ij} = \gamma_w \left(G_s + e^t_{ij} \right) / \left(1 + e^t_{ij} \right)$ = saturated unit weight of element; e^t_{ij} = void ratio of element ij at consolidation time t, and assumed as constant for each time increment; G_s = specific gravity of solid; $\sigma'_{o,ij}$ = signifies initial effective stress; and γ_w = unit weight of pore water. Lateral displacement is neglected, and nodes of each element move vertically during the consolidation process. This approximation of one-dimensional soil strain is valid for most radial consolidation problems, given the large cross-sectional loading area relative to the thickness of compressible layers and the small lateral spacing between PVDs. An additional advantage of this approach is that soil properties derived from standard oedometer tests can be directly used for radial consolidation analysis.

The deviation of hydraulic conductivity in the vertical direction, $k_{z,ij}$, from the original vertical hydraulic conductivity, $k_{v,ij}$, arises due to the distortion of anisotropic soil elements during the consolidation process. This deviation is calculated using the following expression:

$$k^t_{z,ij} = \frac{k^t_{v,ij}}{\sin^2\theta^t_{ij} + \cos^2\theta^t_{ij} / r_k} \tag{7}$$

The vertical volumetric flow rate $q^t_{z,ij}$ between element *ij* and *i,j*+1 is

$$q^t_{z,ij} = -k^t_{zs,ij}\left(i^t_{z,ij}\right)^{\beta} 2\pi r_i d_i \tag{8}$$

where the equivalent vertical series hydraulic conductivity $k^t_{zs,ij}$ is

$$k^t_{zs,ij} = \frac{k^t_{z,ij} k^t_{z,i,j+1}\left(L^t_{ij} + L^t_{i,j+1}\right)}{k^t_{z,ij} L^t_{i,j+1} + k^t_{z,i,j+1} L^t_{ij}} \tag{9}$$

and the vertical hydraulic gradient $i^t_{z,ij}$ is

$$i^t_{z,ij} = \frac{\left(z^t_{i,j+1} + u^t_{i,j+1}/\gamma_w\right) - \left(z^t_{ij} + u^t_{ij}/\gamma_w\right)}{z^t_{i,j+1} - z^t_{ij}} \tag{10}$$

For the upper and bottom elements, $k^t_{zs,i,R_j} = k^t_{v,i,R_j}$ and $k^t_{zs,i,0} = k^t_{v,i,1}$. Non-Darcian flow is incorporated using the exponent β; if Darcy's law is valid, $\beta = 1$.

Analogously, equivalent lateral hydraulic conductivity $k^t_{rs,ij}$, lateral hydraulic gradient $i^t_{r,ij}$ and lateral volumetric flow rate $q^t_{r,ij}$ between element *ij* and *i,j*+1 are

$$k^t_{rs,ij} = \frac{r_k k^t_{v,ij} k^t_{v,i+1,j}\left(d_i + d_{i+1}\right)}{k^t_{v,ij} d_{i+1} + k^t_{v,i+1,j} d_i} \tag{11}$$

(12)
$$i^t_{r,ij} = \frac{\left(z^t_{i+1,j} + u^t_{i+1,j}/\gamma_w\right) - \left(z^t_{ij} + u^t_{ij}/\gamma_w\right)}{\sqrt{\left(d_{i+1} - d_i\right)^2 + \left(z^t_{i+1,j} - z^t_{ij}\right)^2}}$$

(13)
$$q^t_{r,ij} = -k^t_{rs,ij}\left(i^t_{r,ij}\right)^{\beta} 2\pi\left(r_i + \frac{d_i}{2}\right)\left(z^t_{c,ij} - z^t_{c,i,j-1}\right)\sin\theta^t_{ij}$$

For the drain boundary, $k^t_{rs,0,j} = r_k k^t_{sv,1,j}$. The total head varies linearly at the drain. The hydraulic gradient ($i^t_{r,0,j}$) for a fully penetrating drain is computed as follows

(14)
$$i^t_{r,0,j} = \frac{h^t_{1,j} - \left[h_b + \left(h_t - h_b\right)\left(z^t_{c,0,j} + z^t_{c,0,j-1}\right)/\left(2z^t_{c,0,R_{jT}}\right) + \Delta p^t_j/\gamma_w\right]}{\sqrt{\left(d_1/2\right)^2 + \left[z^t_{1,j} - \left(z^t_{c,0,j} + z^t_{c,0,j-1}\right)/2\right]^2}}$$

Once vertical and lateral volumetric flow rates are known, new element volumes are calculated for time $t + \Delta t$ as

(15)
$$V^{t+\Delta t}_{ij} = V^t_{ij} + \left(q^t_{z,i,j-1} - q^t_{z,ij} + q^t_{r,i-1,j} - q^t_{r,ij}\right)\Delta t$$

A new height is calculated for each soil layer over time increment Δt,

(16)
$$H^{t+\Delta t} = \frac{\sum_{i=1}^{R_i}\sum_{j=1}^{R_j} V^{t+\Delta t}_{ij}}{\pi\left(r_e^2 - r_w^2\right)}$$

the settlement profile at time $t + \Delta t$, $S^{t+\Delta t}_i$, is calculated as

(17)
$$S^{t+\Delta t}_i = H_o - z^{t+\Delta t}_{c,i,R_j}$$

and the average settlement of the soil column $S^{t+\Delta t}_{avg}$ is determined by

(18)
$$S^{t+\Delta t}_{avg} = \frac{\sum_{i=1}^{R_i}\sum_{j=1}^{R_j}\left(V_{o,i} - V^{t+\Delta t}_{ij}\right)}{\pi\left(r_e^2 - r_w^2\right)}$$

Random Field

Three natural soil properties, including plasticity index I_p, liquid limit w_L, and initial void ratio e_o, are defined as random variables in this study. These parameters can be efficiently measured through conventional laboratory procedures with well-established protocols, making them particularly advantageous for field investigations and quality control. Their measurability, combined with strong correlations to engineering behavior (Wroth and Wood 1978), ensures these variables are both theoretically significant and practically applicable in probabilistic analysis. A lognormal probability distribution is employed to characterize these random variables, ensuring they remain positive, as required (Huang et al. 2010; Zhu and Zhang 2013).

The probability density function of the random variables is characterized by the autocorrelation length (θ) in both the lateral and vertical directions, the standard deviation (σ), the mean value (μ), and the dimensionless coefficient of variation ν is

(19) $$\nu = \frac{\sigma}{\mu}$$

Extensive research has demonstrated that soil consolidation properties exhibit strong correlations with plasticity index, liquid limit and void ratio. These relationships are well established, as the parameters fundamentally influence soil compressibility, permeability, and time-dependent settlement behavior (Nagaraj and Srinivasa Murthy 1986; Sridharan and Nagaraj 2005; Hong et al. 2012; Shimobe and Spagnoli 2022). For instance, soils with higher plasticity indices and liquid limits typically exhibit greater compressibility due to their higher clay content and associated water-holding capacity. Once I_p, w_L, and e_o in the soil column are known, the consolidation parameters, including compression index C_c, secondary compression coefficient $C_{\alpha e}$ and coefficient of permeability in the vertical direction k_v are computed using the evolutionary polynomial regression method (Jin and Yin 2020), as follows:

(20-a) $$C_c = g\left(I_p, w_L, e_o\right) + a_o$$

$$C_{\alpha e} = f\left(I_p, w_L, e_o\right) + a_1 \tag{20-b}$$

$$k_v = K\left(I_p, w_L, e_o\right) + a_2 \tag{20-c}$$

where a_o, a_1 and a_2 = constants. The variables of interest are assumed to follow a lognormal distribution, meaning that the natural logarithms of these variables are normally distributed (Zhu and Zhang 2013). The standard deviation and mean of the underlying normal distribution for a variable m (i.e., C_c, $C_{\alpha e}$ and k_v) are

$$\sigma_{\ln m} = \sqrt{\ln\left(1 + v_m^2\right)} \tag{21}$$

$$\mu_{\ln m} = \ln \mu_m - \frac{1}{2}\sigma_{\ln m}^2 \tag{22}$$

The inter-variable correlations matrix $\boldsymbol{\rho}$ describes the correlations between the three variables, and is defined as

$$\boldsymbol{\rho} = \begin{bmatrix} 1 & \rho_{12} & \rho_{13} \\ \rho_{21} & 1 & \rho_{23} \\ \rho_{31} & \rho_{32} & 1 \end{bmatrix} \tag{23}$$

The inter-variable correlation matrix is decomposed into the product of a lower triangular matrix and its transpose using Cholesky decomposition.

$$\boldsymbol{\rho} = \mathbf{L}_2 \cdot \mathbf{L}_2^{\mathrm{T}} \tag{24}$$

A single exponential autocorrelation function is adopted to represent the spatial correlation between two points, such as point p (r_p, z_p) and point q (r_q, z_q). This function is widely used in probabilistic analysis due to its computational simplicity.

$$\rho_{pq} = \exp\left[-2\left(\frac{\left|r_p - r_q\right|}{\theta_r} + \frac{\left|z_p - z_q\right|}{\theta_z}\right)\right] \tag{25}$$

where θ_r = autocorrelation length in the lateral direction, and θ_z = autocorrelation length in the vertical direction.

Matrix $\mathbf{L}_2$ is used to transform uncorrelated samples into samples that exhibit the desired inter-variable correlations. Similarly, a Cholesky decomposition is applied to the spatial correlation matrix $\square$ to obtain another lower triangular matrix $\mathbf{L}_1$.

$$\square = \mathbf{L}_1 \cdot \mathbf{L}_1^{\mathrm{T}} \tag{26}$$

The transformation to introduce spatial and inter-variable correlations

$$\square = \mathbf{L}_1 \boldsymbol{U} \mathbf{L}_2^{\mathrm{T}} \tag{27}$$

where $\boldsymbol{U}$ = matrix of uncorrelated standard normal random variables. Transform the correlated normal random field $\square_n$ into a log-normal field with specified mean μ and variance σ^2

$$m_n = \exp\left(\mu_{\ln m_n} + \sigma_{\ln m_n} \square_n\right) \tag{28}$$

A flowchart illustrating the basic algorithm for the calculation loop is shown in Fig. 3. The required input data for a simulation include the number of elements (R_i and R_j), the applied stress or pressure conditions (e.g., σ'_o, Δq and Δp), the specific gravity of the solid particles (G_s), the boundary drainage conditions, and parameters for the constitutive relationships (compressibility and hydraulic conductivity). The consolidation calculation model is embedded in Monte Carlo simulations for probabilistic analysis. N_f groups of R_j random values are generated, and the values from each group are assigned to the corresponding elements in one Monte Carlo simulation, where N_f is the total number of simulations. A minimum number of simulations is typically required to obtain accurate results, and this number depends on the total number of random variables involved (Bari 2012). After RCS-EVP reads the input data, an initial calculation is performed to determine the initial configuration for each element, including L_o, d_i, $V_{o,ij}$, and $z_{o,ij}$. To begin the main calculation loop, the elevation and total stress are computed for each node. The distribution of total head is then used to compute flow between contiguous elements, and the vertical compression of each element is calculated from the net fluid outflow during the time increment Δt. Updated element volumes, void ratios, and their changes are calculated, along with the settlement profile and the average settlement. The variation in void ratio for each element is used to calculate changes in effective stress using Eq. (5). Program execution terminates when $t \geqslant t_f$, where t_f is a user-specified final value. If the termination condition is not satisfied, RCS-EVP repeats the calculation sequence with updated values of e_{ij}, V_{ij}, and H.

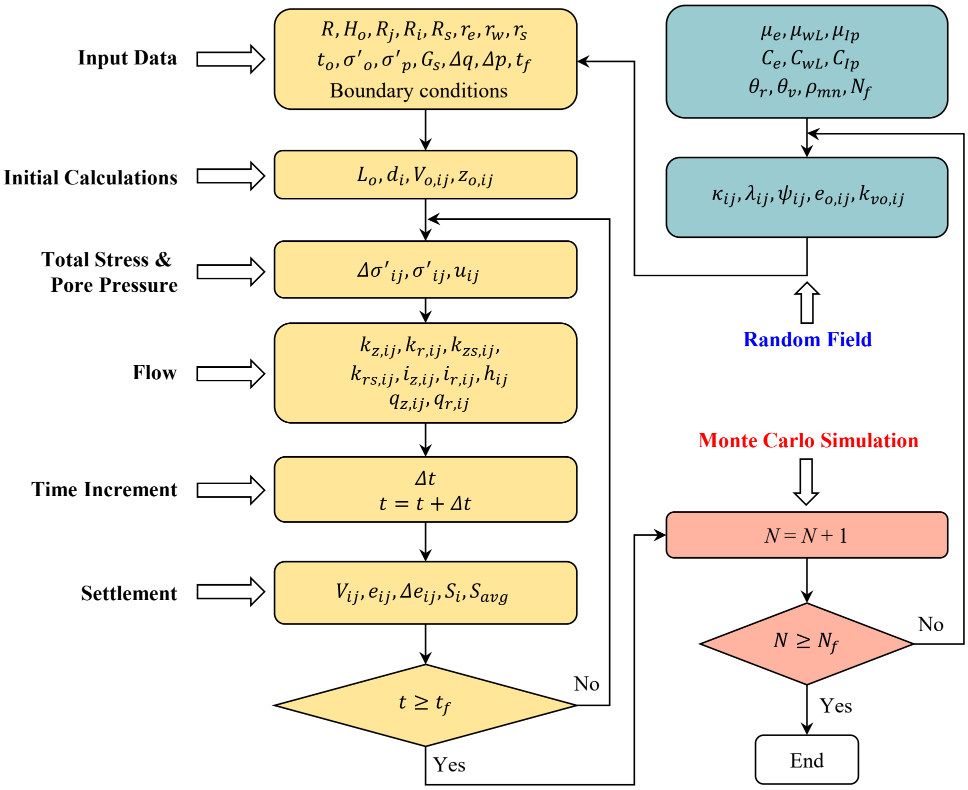

Fig. 3. Flow chart for the probabilistic analysis of the radial consolidation using RCS-EVP

Field Case

The Minmi to Beresfield extension of Sydney-Newcastle Freeway was constructed by the Roads and Traffic Authority (RTA) of New South Wales (NSW), approximately 150 km north of Sydney (Lo et al. 2008). This extension includes a 300 m embankment, referred to as the Leneghans embankment, which was built over a soft clay foundation with a water content ranging from 72% to 99%. Due to the soft, compressible nature of these clay deposits, several design measures were implemented to improve embankment stability and to minimize post-construction settlement to acceptable limits. These measures included lightweight fill using bottom ash, prefabricated vertical drains, surcharging and staged construction. One unique feature of this embankment project is the long-term monitoring of ground movement; settlement profiles at the foundation level were systematically recorded over a period of 9 years.

Prior to construction, a series of boreholes were drilled to investigate subsurface conditions. The underlying subsoil primarily consists of very soft to soft alluvial clay extending to a depth of 16 m (H_o = 16 m). This clay layer, with a high-water content near its liquid limit, showed a liquid limit of 82% to 94%, a plastic limit of 28% to 31%, a plasticity index of 54% to 63%, and an organic content of 2% to 6%, classifying it as high plasticity clay (CH) with a saturated unit weight of 14.8 to 16.2 kN/m^3.

To accelerate the consolidation process, PVDs were installed through the full depth of the soft clay layer at 1.5 m intervals in a triangular pattern. Each PVD has nominal dimensions of 100 mm in width by 4 mm in thickness, with a corrugated polyvinyl chloride core and a geotextile filter. The inner and outer radii of the clay cylinder associated with each PVD are 0.033 m and 0.80 m, respectively. The discharge capacity of the PVDs, q_w, was tested to exceed 11×10^{-6} m^3/s under a hydraulic gradient of 1 (over 346 m^3/year), with a confining stress that simulates the maximum in-situ stress but not less than 200 kPa. Drain flow resistance can be ignored when the q_w exceeds 100-150 m^3/year, and thus well resistance is not taken into account in RCS-EVP simulations. Installation of PVDs was carried out using a mandrel system designed to minimize disturbance and smearing of the surrounding soft clay. RCS-EVP simulations follow the recommendations by Bergado et al. (1991) and Hansbo (1993), applying an $r_s/r_w = 2$ and $\eta = r_k$ (i.e., $k_{rs} = k_v$) to model the soil smear.

The compressibility and hydraulic conductivity of soft soils are strongly correlated with basic physical properties, such as Atterberg limits and void ratio. In this study, predictive models developed by Jin et al. (2009) and Jin and Yin (2020) were employed to determine key soil parameters for constitutive relationships, including λ, ψ, and k_v.

$$\lambda_{ij} = \left[0.3206 e_{o,ij} w_{L,ij} - 0.0284 e_{o,ij} \left(w_{L,ij} I_{p,ij} \right)^2 + 0.0213 \left(e_{o,ij} w_{L,ij} I_{p,ij} \right)^2 - \frac{0.1412 \left(w_{L,ij} \right)^2}{I_{p,ij}} - 0.0540 \left(e_{o,ij} \right)^2 w_{L,ij} I_{p,ij} + 0.6689 \right] / \ln 10 \tag{29}$$

$$\psi_{ij} = \left[\exp\left(0.9092 \frac{c_l^2}{w_{L,ij} I_{p,ij}} + 0.6283 \frac{c_l^2}{w_{L,ij} I_{p,ij}} - 10.3212 \left(I_{p,ij} c_l \right)^2 - 0.1963 \left(\frac{c_l}{w_{L,ij} I_{p,ij}} \right)^2 + 3.9741 \left(I_{p,ij} \right)^2 \right) e_{o,ij} - 6.0928 \right] / \ln 10 \tag{30}$$

$$\log k_{v,ij} = \left(-1.0334 I_{p,ij} + 0.9435 \frac{w_{L,ij}^2}{I_{p,ij}} + \frac{0.0762}{w_{L,ij} I_{p,ij}} \right) e_{ij} - 10.409 \quad \left(m/s \right) \tag{31}$$

where c_l = clay content of soil and assumed a constant 0.27 in this case. Terzaghi (1943) and Yin (2015) reported the ratio of κ/λ fall in the range from 0.02 to 0.2, and a value of 0.08 within this range was adopted for analysis. The hydraulic conductivity anisotropy was modelled using $r_k = 2$ (i.e., $k_r/k_v = 2$). Based on the quantitative relationship between shear strength and over-consolidation ratio established by Potts and Ganendra (1991), Lo et al. (2008) derived the distribution of pre-consolidation pressure σ'_p within soil profiles from measured shear strength, as illustrated in Fig. 4(a). This study adopts the assumptions of initial and reference stress (σ'_o and σ'_{ro}) in soil profiles presented by Lo et al. (2008), as shown in Fig. 4(a), as well as a time-dependent surcharge loading schedule (Fig. 4b) reflecting the three-stages fill placement history.

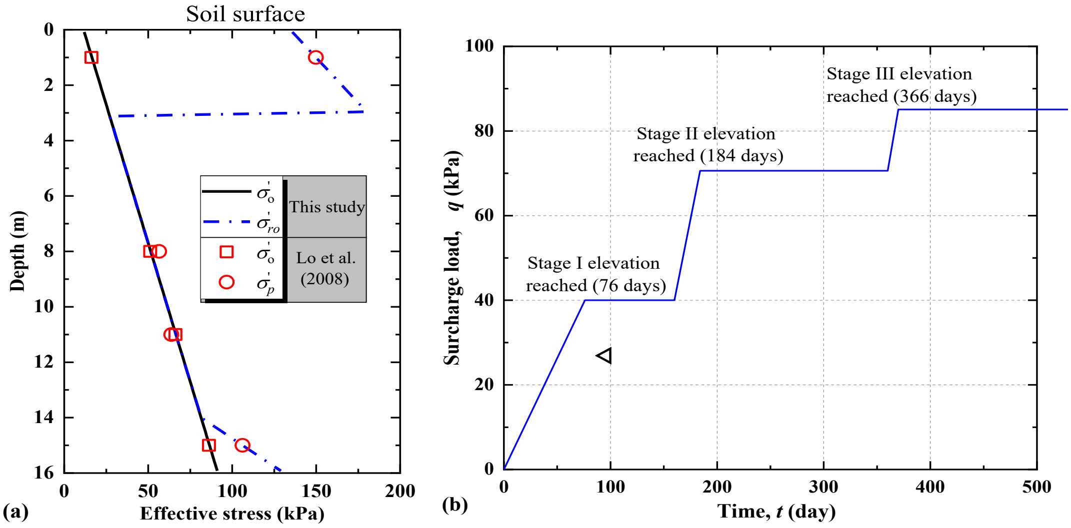

Fig. 4. Input parameters for numerical simulations: (a) distributions of σ'_o and σ'_{ro}; and (b) surcharge stress versus time

Random field for e_o, w_L and I_p are generated using average values of 2.3, 88% and 58% according to a measured liquid limit from 82% to 94% and plasticity index from 28% to 31% by Lo et al. 2008. Due to limited statistical data in Lo et al. (2008), additional statistical assumptions were made according to typical values reported in current studies (Phoon and Kulhawy 1999; Phoon and Ching 2012). A relatively low coefficient of variation (ν = 0.03) was adopted, as preliminary analyses indicated that higher COVs significantly increased computational costs and often caused convergence issues due to highly nonlinearity between physical properties and constitutive parameters. Cross-correlations among the random variables were incorporated as current studies (Spagnoli et al. 2018) reported a strong correlation between liquid limit and plasticity index, with plasticity index increasing as liquid limit increases. In contrast, the initial void ratio and Atterberg limits show weaker, indirect correlations. However, high-plasticity clays often have higher natural void ratios due to their plate-like particle structure and water retention. Accordingly, a high value of ρ_{w_L,I_p} (= 0.5) was used, and lower values of 0.1 were used for ρ_{e_o,w_L} and ρ_{e_o,I_p}. Autocorrelation lengths were assumed as θ_r = 2 m for lateral direction and θ_z = 20 m for vertical direction.

Probabilistic Analysis Results

Fig. 5 presents the settlement results of a soil column over time, derived from N_f = 1000 Monte Carlo simulations using the RCS-EVP, as well as field measurements (represented by black dots) for comparison. The simulations account for spatial variability in critical soil parameters, such as compressibility and hydraulic conductivity, which significantly influence settlement behavior. The spread of simulation results reflects inherent variability arising from spatial heterogeneity in soil properties, which is crucial for estimating the range of potential settlements. The simulated settlement curves exhibit strong agreement with the measured data, demonstrating the model's capability to accurately capture the overall settlement trend. The alignment of measured values within the simulated range indicates that the model parameters and assumptions effectively represent the underlying soil mechanics. Preliminary simulations were performed using N_f = 100, 500, 1000, 1500, and 2000. By comparing settlement density distributions and average settlement values at selected time points (e.g., t = 100, 500, 1000, and 3000 days), the optimal value of N_f was identified, following a method similar to that used by Bari (2012). The results show that outcomes for $N_f \geq 1000$ are nearly identical. Considering both computational efficiency and accuracy, N_f = 1000 was adopted for simulations. Fig. 6 illustrates the probability density distribution of settlement at 100, 1000, 2000, and 3000 days, derived from the RCS-EVP simulations. Each subplot includes a histogram of observed settlement values overlaid with a probability density function, highlighting the variability and likelihood of settlement outcomes over time. From 100 to 3000 days, the distributions evolve markedly in both central tendency and spread. At 100 days, the distribution is narrowly centered around 0.17 m, indicating low variability and a consistent early-stage response. By 1000 days, the central values shift to around 1.40 m, with a broader distribution reflecting increased spatial heterogeneity during consolidation. At 2000 days, the distribution centers near 1.63 m and remains wide due to continued consolidation. By 3000 days, the distribution consolidates around 1.73 m with reduced variability, closely aligning with the measured value of 1.66 m. The strong correspondence between the measured settlements and the peaks of the distributions, evidenced by the alignment of means, medians, and modes, demonstrates the effectiveness of the probabilistic consolidation analysis framework. Moreover, associated strains increase from 1.06% at 100 days to 10.39% at 3000 days, indicating substantial deformation. The narrowing distribution in later stages suggests convergence toward a more predictable long-term settlement state.

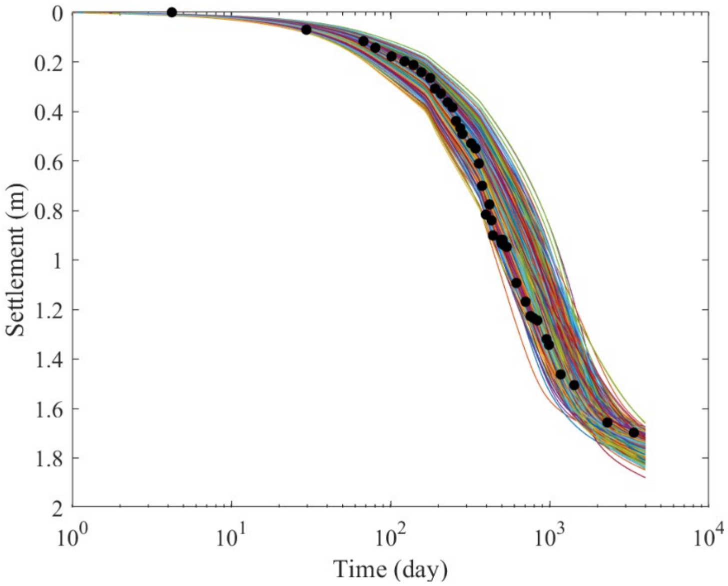

Fig. 5. Simulation results of settlement curves

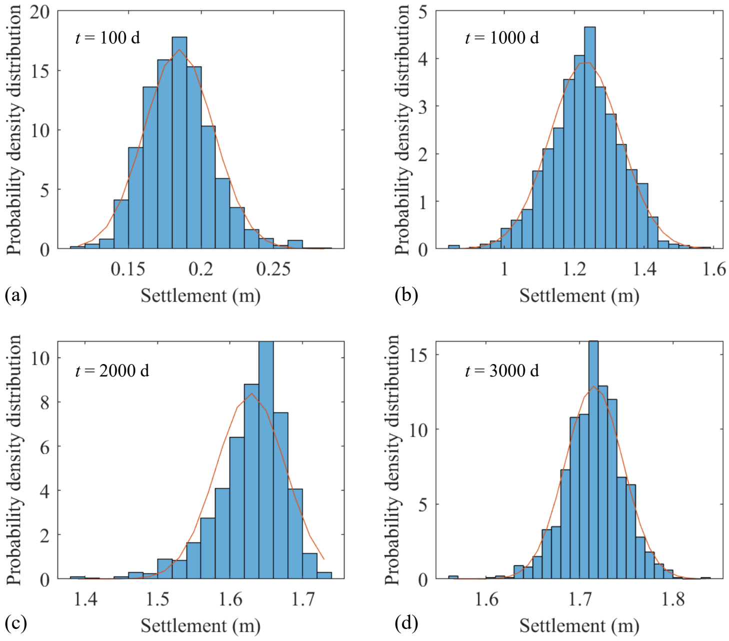

Fig. 6. Probability density distributions at specific time points

During field monitoring, pneumatic piezometers were installed at the midpoints between the PVDs (i.e., at locations near the outer boundary of the unit cell shown in Fig. 1) along several instrumentation lines and at various depths. Expected excess pore pressure measurements were recorded at two elevations on the two instrumentation lines, approximately at z_o = 8.3 m and 13.8 m, as summarized and presented by Lo et al. (2008). These measurements are represented as scatter points in Fig. 7, where data corresponding to the same elevation represent distinct soil profiles. The measured results reveal significant variations in excess pore pressures at the same elevation, likely due to the inherent spatial variability of soil parameters, particularly hydraulic conductivity. The observed trends are consistent with the applied stress sequence shown in Fig. 4(b), excess pore pressure increases during the staged construction process and decreases once corresponding fill elevation is reached. Measurements taken at higher elevations exhibit lower excess pore pressure values, as these locations are closer to the sand blanket, which serves as a free-draining boundary. The simulation results show a similar pattern. Simulated excess pore pressures at lower elevations exhibit a broader distribution after completion of Stage III fill, likely due to their greater distance from the drainage boundary, which results in delayed dissipation of excess pore pressure. This delayed response is sensitive to spatial variations in hydraulic conductivity and aligns with the findings of Song et al. (2023b) for the uncertainty analyses of one-dimensional consolidation. Moreover, Huang et al. (2023) reported that several factors complicate the calibration of simulated and measured pore pressures, including potential clogging of the vertical drain filter tip, changes in the static water table due to rainfall, sensor movement, and soil inhomogeneity. Consequently, the potential error in pore pressure measurements may be greater than in settlement data.

Measured and simulated excess pore pressures at the two locations are compared in Fig. 7. The measured results fall within the range of simulated outcomes, indicating that probabilistic analysis using the RCS-EVP model, while accounting for spatial variability in soil parameters, provides a robust framework for estimating the long-term settlement behavior of soft soils with PVDs. This approach improves both the reliability and robustness of consolidation modeling.

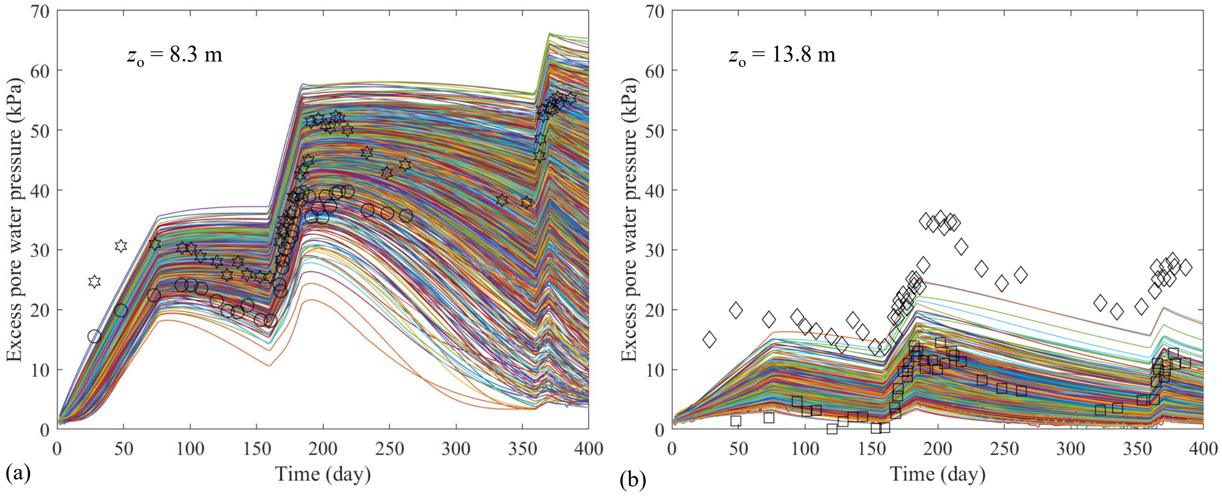

Fig. 7. Relationships of excess pore pressure versus time for z_o = 8.3 m and z_o = 13.8 m

Coefficient of Variation

Huang et al. (2010) performed parametric studies in which the coefficients of volume compressibility and permeability were varied from 0.125 to 4.0 times their baseline values, noting that these parameters were occasionally pushed to particularly high levels. In the present study, the influence of the coefficient of variation on the probabilistic analysis of radial consolidation was investigated using relatively low values, ν = 0.01, 0.03 and 0.05. Results for ν = 0.03 are shown in Figs. 5-7, while those for ν = 0.01 and 0.05 are shown in Fig. 8. For ν = 0.01, the settlement curves are tightly clustered, indicating low variability in the simulated settlement results. Conversely, for ν = 0.05 shows a broader spread of settlement outcomes, reflecting increased variability in the estimates. A lower coefficient of variation results in more precise, though not necessarily more accurate estimations, while a higher coefficient of variation captures a broader range of possible scenarios. This indicates more consistent settlement behavior with smaller ν values. Fig. 9 presents the probability density distributions of settlement at selected time points (t = 100, 1000, and 3000 days) for ν = 0.01 and ν = 0.05, respectively. Comparisons of the estimated settlement across different ν values at these points demonstrate that the distribution range increases significantly with higher ν values. Specifically, as ν increases from 0.01 to 0.05, the settlement distribution expands by a factor of five to six, and this expansion exhibits an approximately linear relationship with the ν increase. Cheng et al. (2017) reported that the mean settlement decreases significantly with a reduction in the coefficient of variation for consolidation of one-dimensional unsaturated soil. However, this trend was not observed in present study, likely because a nonlinear constitutive model was adopted here, whereas Cheng et al. (2017) employed a linear-elastic model.

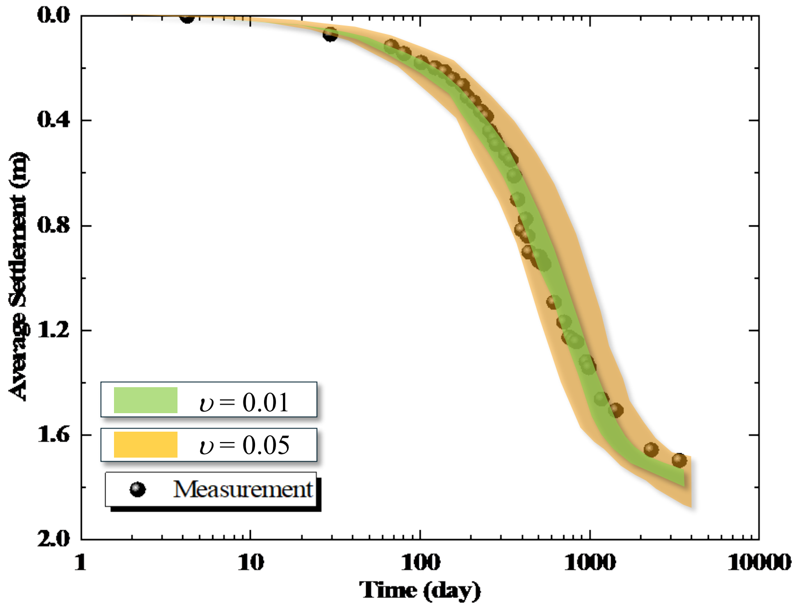

Fig. 8. Comparison of settlements for various coefficient of variation

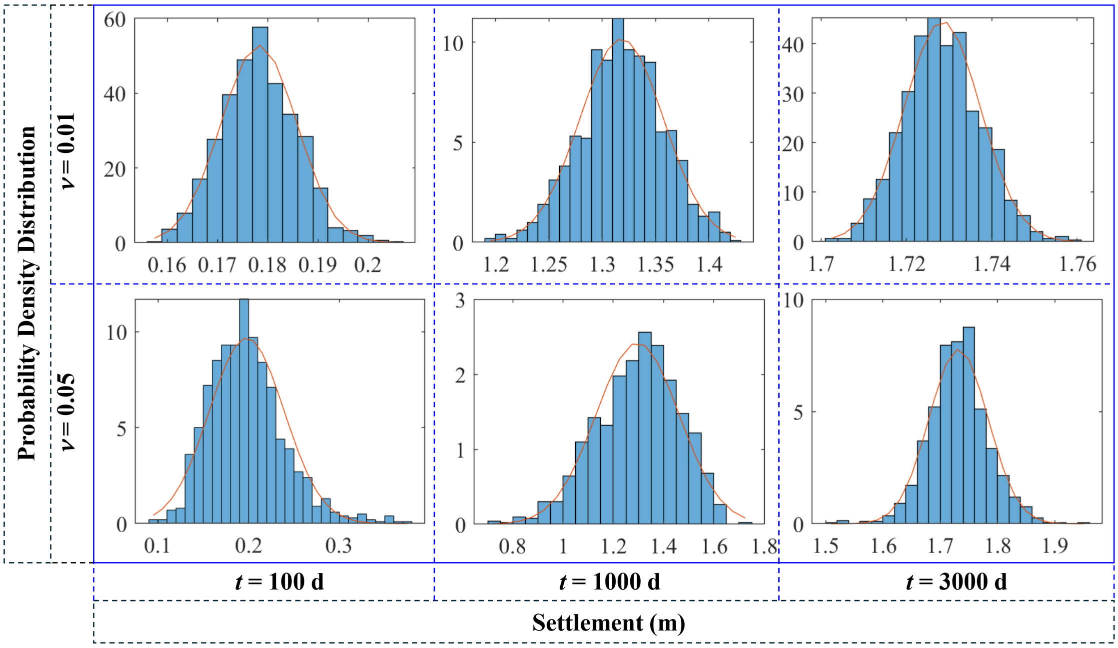

Fig. 9. Comparison of probability density distributions for various coefficient of variation

Estimated excess pore pressure curves for ν = 0.01 and 0.05 at depths of z_o = 8.3 m and 13.8 m are shown in Fig. 10. Similar to the trend observed in the settlement results, a significantly wider range of estimated excess pore pressures is observed in simulations with a larger coefficient of variation. For ν = 0.01, some measured excess pore pressures fall outside the range of simulated results, indicating that these simulations underestimate the spatial variability of soil parameters. In contrast, simulations with ν = 0.05 slightly overestimate the spatial variability. Based on these observations, the coefficient of variation for the clay layer in the field case is likely in the range of 0.03 to 0.05.

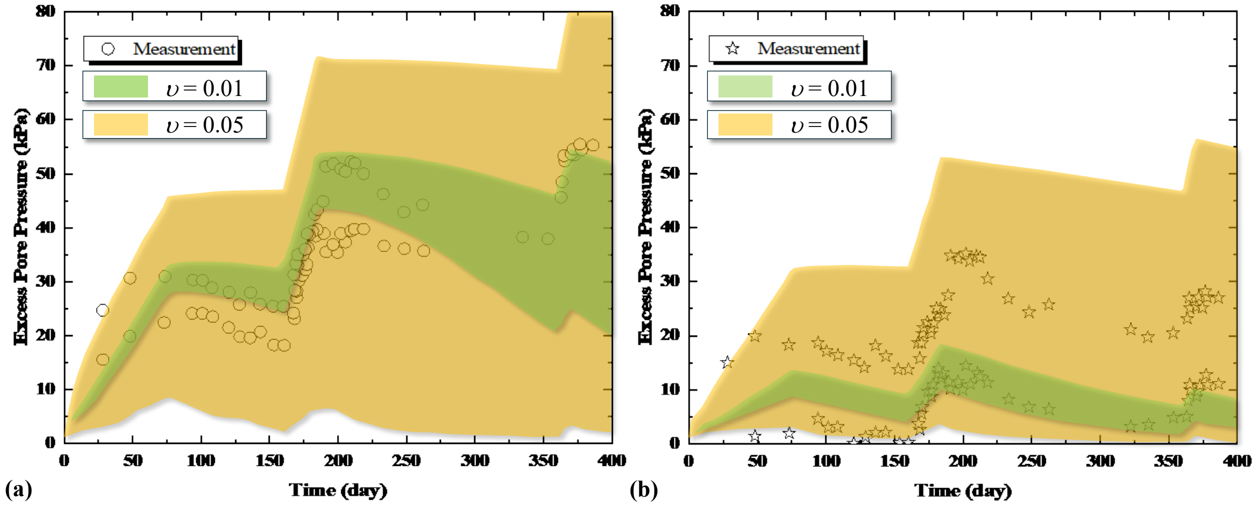

Fig. 10. Excess pore pressures comparison for various coefficient of variation for (a) $z_o = 8.3$ m and (b) $z_o = 13.8$ m

Autocorrelation Distance

Two more Monte Carlo simulations were conducted using $\theta_{\ln,v} = 12$ m, $\theta_{\ln,h} = 1.2$ m and $\theta_{\ln,v} = 32$ m, $\theta_{\ln,h} = 3.2$ m to investigate the effects of autocorrelation distances in the vertical ($\theta_{\ln,v}$) and lateral ($\theta_{\ln,h}$) directions. All other parameters were consistent with those used in the Field Case section. Plots of settlements for simulations with different $\theta_{\ln,v}$ and $\theta_{\ln,h}$ values are shown in Fig. 11, while the probability density distributions at selected time points ($t = 100$, 1000, and 3000 days) are presented in Fig. 12. Increasing the autocorrelation distance ($\theta_{\ln,v}$ and $\theta_{\ln,h}$) results in a slightly larger range of simulated settlements. However, measured settlement values remain within the range of simulated results, even for smaller $\theta_{\ln,v}$ and $\theta_{\ln,h}$ values. This suggests that autocorrelation distances may not significantly influence the probability analysis of consolidation settlement, especially when compared to the effects of the coefficient of variation. Interestingly, simulations using vertical autocorrelation distances ($\theta_{\ln,v} = 20$ m and $\theta_{\ln,v} = 32$ m) larger than the initial height of the soil column ($H_o = 16$ m) show no significant impact on the estimated consolidation settlement.

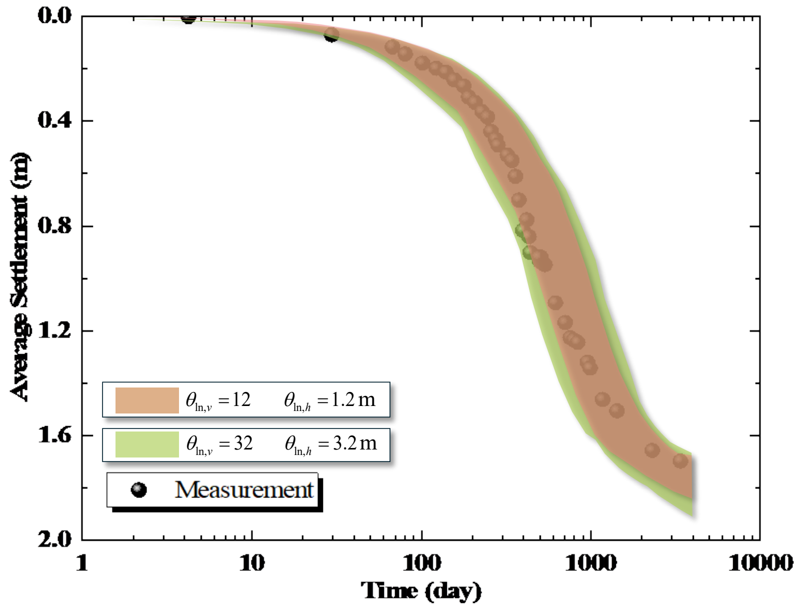

Fig. 11. Comparison of settlements for various autocorrelation distance

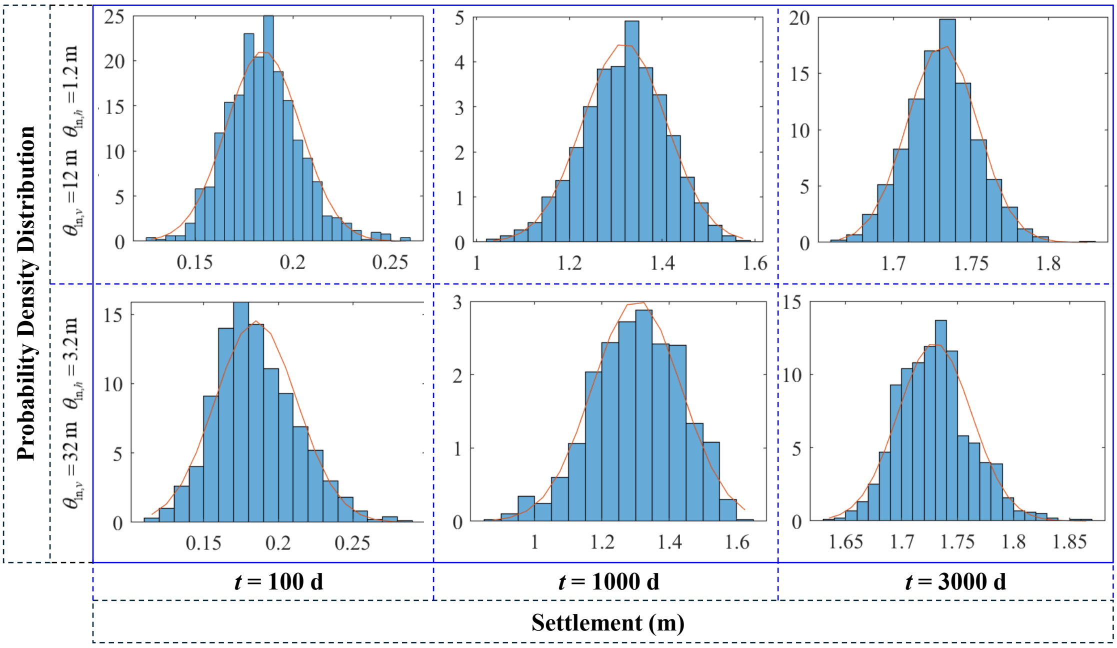

Fig. 12. Comparison of probability density distributions for various autocorrelation distance

Fig. 13 illustrate estimated excess pore pressure curves for $\theta_{\ln,v}$ = 12 m, $\theta_{\ln,h}$ = 1.2 m and $\theta_{\ln,v}$ = 32 m, $\theta_{\ln,h}$ = 3.2 m at depths of z_o = 8.3 m and 13.8 m. With increasing autocorrelation distances, only a slight increase in the range of the estimated excess pore pressure values is observed, consistent with the trends seen for the effects of autocorrelation distances on consolidation settlement. Most of the measured values fall within the simulated range for various autocorrelation distances. This suggests that autocorrelation distances have minimal influence on the probability analysis of excess pore pressure dispersion during the consolidation process. Bari et al. (2016) conducted a probabilistic analysis of radial consolidation for both single-drain and multi-drain systems and stated that stochastic equivalence between the unit cell and multi-drain solutions can be established by assigning appropriate representative point statistics for the idealized unit cell. These statistics can be computed from the statistical parameters assigned to the multi-drain by using appropriate transformation method, ensuring that their underlying local average statistics remain consistent. In the present study, a single-drain system was used, and results indicate that autocorrelation distances have limited impact on the mean and variability of consolidation characterizes. Using a single-drain system for probabilistic analysis is feasible (Bari et al. 2016) and offers improved computational efficiency. Although autocorrelation distance is not a dominant factor in the analysis, it can influence other statistical parameters, e.g., such as the coefficient of variation, during practical data collection. This is of particular concern as the coefficient of variation has a significant effect on the consolidation analysis.

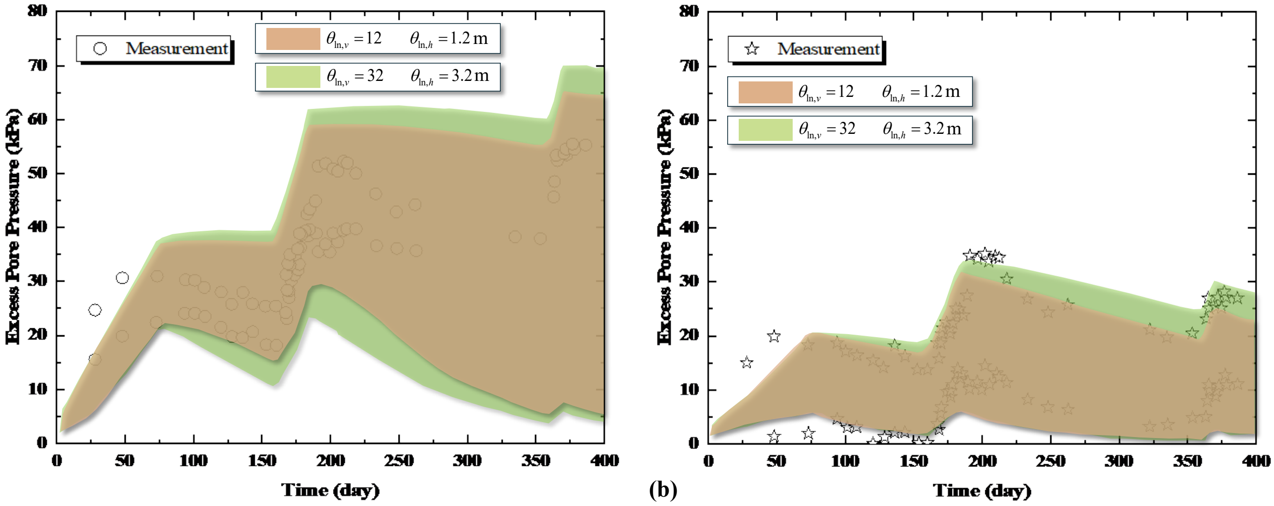

Fig. 13. Excess pore pressures comparison for various autocorrelation distance for (a) z_o = 8.3 m and (b) z_o = 13.8 m

Cross-correlation Coefficient

The effect of cross-correlation coefficient on the probabilistic analysis of consolidation process was investigated for the same case using $\rho_{e_o,w_L} = \rho_{e_o,I_p} = 0.05$, $\rho_{w_L,I_p} = 0.25$ and $\rho_{e_o,w_L} = \rho_{e_o,I_p} = 0.2$, $\rho_{w_L,I_p} = 0.75$, with all other parameters kept unchanged. Fig. 14 shows plots of settlements for simulations with different cross-correlation coefficients, while Fig. 15 illustrates the probability density distribution of simulated settlements at $t = 100$, 1000, and 3000 days. Similar to the effects of autocorrelation distance, the range of simulated settlements increase slightly with higher values of cross-correlation coefficient. However, the influence of the cross-correlation coefficient on the probability analysis of consolidation settlement is somewhat more significant than that of autocorrelation distance but less influential than that of the coefficient of variation.

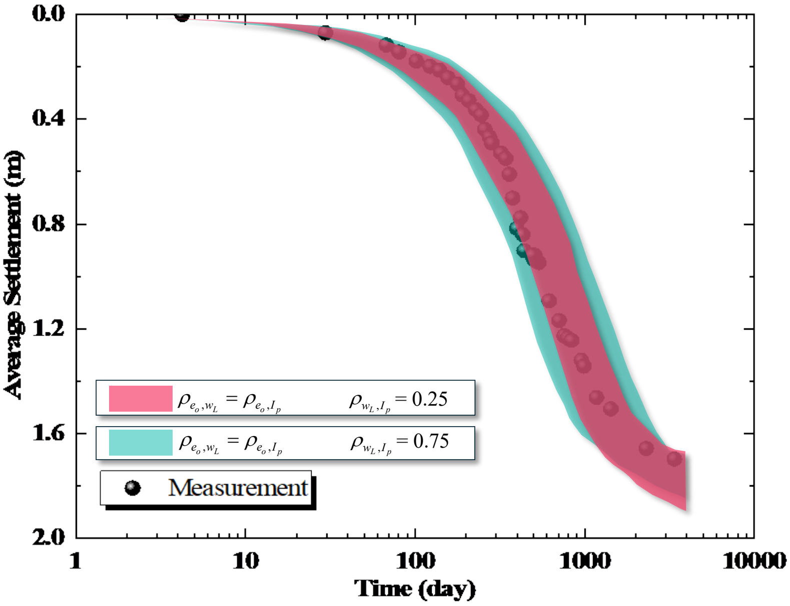

Fig. 14. Comparison of settlements for various cross-correlation coefficient

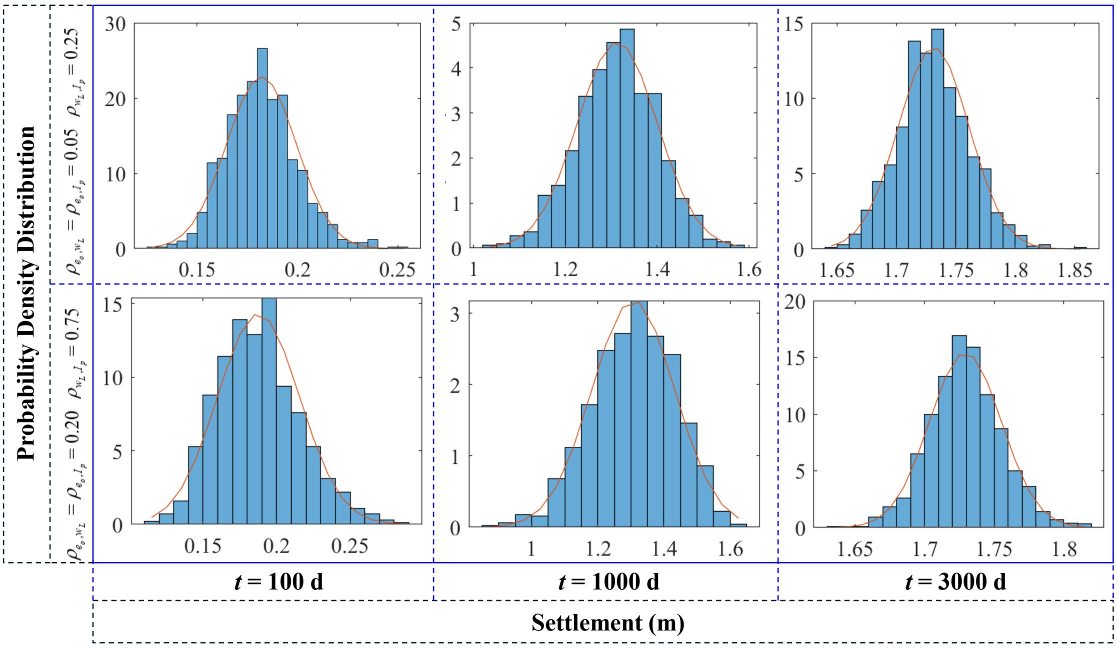

Fig. 15. Comparison of probability density distributions for cross-correlation coefficient

Simulated excess pore pressure for $\rho_{e_o,w_L} = \rho_{e_o,I_p}$ = 0.05, ρ_{w_L,I_p} = 0.25 and $\rho_{e_o,w_L} = \rho_{e_o,I_p}$ = 0.2, ρ_{w_L,I_p} = 0.75 at depths of z_o = 8.3 m and 13.8 m are illustrated in Fig. 16. A very limited increase in the range of simulated excess pore pressures was observed with increasing cross-correlation coefficients, consistent with the trend of the effects of ρ on consolidation settlement. The estimated excess pore pressures encompass the distribution patterns of measured values, indicating that cross-correlation coefficients have no significant influence on the dispersion of excess pore pressure within the soil column. Thus, the coefficient of variation has the most significant influence on the probability analysis framework for large-strain, long-term radial consolidation, aligning with the findings of Houmadi et al. (2012) for one dimensional elastic consolidation. Bari (2012) reported that with higher cross-correlation between the permeability coefficient and the coefficient of volume compressibility, the evolution of excess pore dispersion is slower, resulting in lower rates of change in both the mean and standard deviation. In the present study, higher cross-correlation coefficients led to a larger deviation in the consolidation rate, while the mean values remained nearly constant.

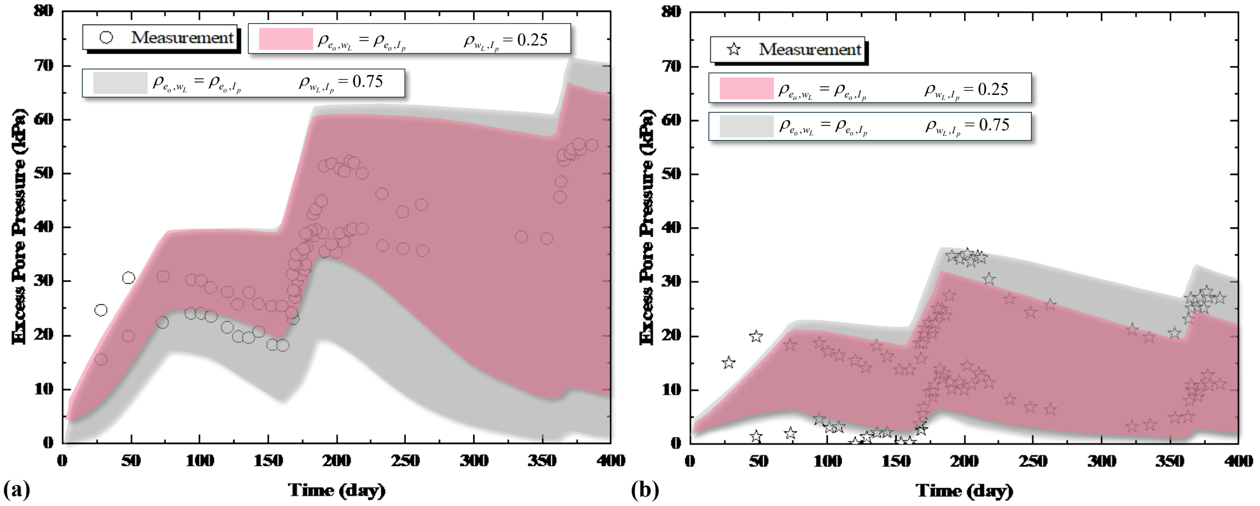

Fig. 16. Excess pore pressures comparison for various cross-correlation coefficient for (a) z_o = 8.3 m and (b) z_o = 13.8 m

This study advocates the adoption of void ratio (*e*), plastic index (PI), and liquid limit (LL) as random parameters for characterizing soil spatial variability. These indices are routinely measured during site investigations, enabling robust statistical characterization without imposing additional field testing burdens. Although few studies have focused on using these parameters as stochastic descriptors their widespread availability facilitates the derivation of critical statistics, including mean values and coefficients of variation. Although *e*, PI, and LL exhibit strong correlations with compressibility and permeability properties, their quantitative relationships remain subject to site-specific uncertainties. Empirical correlations between these indices and consolidation parameters require further validation across diverse soil types and depositional environments. Nevertheless, their use offers distinct advantages over direct randomization of permeability coefficient or coefficient of volume compressibility, particularly given the inherent challenges in field determination of consolidation properties due to sampling disturbances. In addition, it is worth further consideration that the installation of PVDs may alter the statistical characteristics of the random variables, particularly with respect to the variability between the smear zone and undisturbed zone, as well as their potential correlation.

A sensitivity analysis reveals that among the three stochastic descriptors, including coefficient of variation, autocorrelation distance, and cross-correlation coefficient, only coefficient of exerts a statistically significant influence on radial consolidation probability outcomes. This underscores the necessity of prioritizing cost-effective and accurate estimation of the coefficient of variation during field data collection and statistical inference. Refining these estimates through high-resolution sampling or Bayesian updating techniques is important, as mischaracterization of this parameter may lead to non-conservative reliability predictions.

Conclusions

The following conclusions are reached as a result of this study of probability analysis of large strain long-term radial consolidation of soft soils:

1. A probabilistic analysis framework for coupled long-term consolidation of soft soils incorporating prefabricated vertical drains was developed using a piecewise-linear approach and an elastic visco-plastic constitutive relationship. This framework accounts for spatial variability in soil parameters (including compressibility and hydraulic conductivity), creep strain, large-strain effects, hydraulic conductivity anisotropy, vertical and radial flows, soil smear, time-dependent loading, and variable hydraulic conductivity and compressibility during the consolidation process. Three naturally measured soil parameters, including plasticity index, liquid limit and void ratio, were selected as random variables due to their ease of on-site measurement. Spatial variation of soil constitutive parameters was determined using relationships derived from these random variables.
2. The probabilistic analysis framework was used to model radial consolidation for a preloaded site on the Sydney-Newcastle Freeway in New South Wales. An underlying 16 m-thick layer of soft clay is a potential source of long-term large settlements for the site. Prefabricated vertical drains were installed in the soft clay layer to accelerate consolidation in the surcharged

areas. Field measurements of settlement and excess pore pressure were found to fall within the range of simulated results, demonstrating that the framework effectively captures the long-term settlement process.

3. The coefficients of variation for spatial soil parameters significantly influence both settlement and excess pore pressures, with higher coefficients producing a wider range of estimated values. Similar trends were observed for the effects of autocorrelation distances (in both vertical and lateral directions) and cross-correlation coefficients, although their impact on the probability analysis of the consolidation process was considerably weaker.

CRediT Authorship Contribution Statement

Ding-Bao Song: Writing original draft, Visualization, Methodology, Software, Investigation. **Zhen-Yu Yin**: Writing – review & editing, Resources, Data curation, Funding acquisition. **Jian-Hua Yin**: Writing – review & editing, Resources, Funding acquisition, Supervision.

Declaration of Competing Interest

The authors declare that they have no known competing financial interests or personal relationships that could have appeared to influence the work reported in this paper.

Data Availability Statement

The data that support the findings of this study are available from the corresponding author upon reasonable request.

Acknowledgments

This research was supported by the Research Grants Council of Hong Kong Special Administrative Region Government of China (Grant No.: R5037-18F, 15210322, and 15226722) and the Research Centre for Resources Engineering towards Carbon Neutrality (RCRE) of The Hong Kong Polytechnical University (Grant No.: 1-BBEM). The authors also acknowledge the finial support from the Environment and Conservation Fund (No. 2023-64) of the Environment Protection Department of Hong Kong. This support is gratefully acknowledged.

References

Baral, P., Indraratna, B., Rujikiatkamjorn, C., Kelly, R., and Vincent, P. 2021. Consolidation by Vertical Drains beneath a Circular Embankment under Surcharge and Vacuum Preloading. Journal of Geotechnical and Geoenvironmental Engineering **147(8)**: 05021004.

Bari, M. W. 2012. Modelling of ground improvement by vertical drains in highly variable soils. Doctoral dissertation, Curtin University, Bentley Western Australia.

Bari, M. W., Shahin, M. A., and Soubra, A. H. 2016. Probabilistic analyses of soil consolidation by prefabricated vertical drains for single‐drain and multi‐drain systems. International Journal for Numerical and Analytical Methods in Geomechanics **40(17)**: 2398-2420.

Bergado, D. T., Asakami, H., Alfaro, M. C., and Balasubramaniam, A. S. 1991. Smear effects of vertical drains on soft Bangkok clay. Journal of Geotechnical Engineering **117(10)**: 1509-1530.

Bergado, D. T., Balasubramaniam, A. S., Fannin, R. J., and Holtz, R. D. 2002. Prefabricated vertical drains (PVDs) in soft Bangkok clay: a case study of the new Bangkok International Airport project. Canadian Geotechnical Journal **39(2)**: 304-315.

Bong, T., Son, Y., Noh, S., and Park, J. 2014. Probabilistic analysis of consolidation that considers spatial variability using the stochastic response surface method. Soils and Foundations **54(5)**: 917-926.

Chai, J. C., Shen, S. L., Miura, N., and Bergado, D. T. 2001. Simple method of modeling PVD-improved subsoil. Journal of Geotechnical and Geoenvironmental Engineering **127(11)**: 965-972.

Cheng, Y., Zhang, L. L., Li, J. H., Zhang, L. M., Wang, J. H., and Wang, D. Y. 2017. Consolidation in spatially random unsaturated soils based on coupled flow-deformation simulation. International Journal for Numerical and Analytical Methods in Geomechanics **41(5)**: 682-706.

Chu, J., Yan, S. W., and Yang, H. 2000. Soil improvement by the vacuum preloading method for an oil storage station. Géotechnique **50(6)**: 625-632.

Geng, X., and Yu, H. S. 2017. A large-strain radial consolidation theory for soft clays improved by vertical drains. Géotechnique **67(11)**: 1020-1028.

Hansbo, S. 1993. Band drains. Ground improvement, M. P. Mosely, ed. Chemical Rubber Corp., Boca Raton, Fla., pp 40-64.

Hong, Z. S., Zeng, L. L., Cui, Y. J., Cai, Y. Q., and Lin, C. 2012. Compression behaviour of natural and reconstituted clays. Géotechnique **62(4)**: 291-301.

Houmadi, Y., Ahmed, A., and Soubra, A. H. 2012. Probabilistic analysis of a one-dimensional soil consolidation problem. Georisk: Assessment and Management of Risk for Engineered Systems and Geohazards **6(1)**: 36-49.

Hu, Y. Y., Zhou, W. H., and Cai, Y. Q. 2014. Large-strain elastic viscoplastic consolidation analysis of very soft clay layers with vertical drains under preloading. Canadian Geotechnical Journal **51(2)**: 144-157.

Huang, J., Griffiths, D. V., and Fenton, G. A. 2010. Probabilistic analysis of coupled soil consolidation. Journal of Geotechnical and Geoenvironmental Engineering **136(3)**: 417-430.

Huang, S., Huang, J., Kelly, R., Jones, M., and Kamruzzaman, A. H. M. 2023. Predicting settlement of embankments built on PVD-improved soil using Bayesian back analysis and elasto-viscoplastic modelling. Computers and Geotechnics **157**: 105323.

Huang, S., Mahadevan, S., and Rebba, R. 2007. Collocation-based stochastic finite element analysis for random field problems. Probabilistic Engineering Mechanics **22(2)**: 194-205.

Indraratna, B., Rujikiatkamjorn, C., Baral, P., and Ameratunga, J. 2019. Performance of marine clay stabilised with vacuum pressure: Based on Queensland experience. Journal of Rock Mechanics and Geotechnical Engineering **11(3)**: 598-611.

Indraratna, B., Zhong, R., Fox, P. J., and Rujikiatkamjorn, C. 2017. Large-strain vacuum-assisted consolidation with non-Darcian radial flow incorporating varying permeability and compressibility. Journal of Geotechnical and Geoenvironmental Engineering **143(1)**: 04016088.

Jin, Y. F., and Yin, Z. Y. 2020. An intelligent multi-objective EPR technique with multi-step model selection for correlations of soil properties. Acta Geotechnica **15(8)**: 2053-2073.

Jin, Y. F., Yin, Z. Y., Zhou, W. H., Yin, J. H., and Shao, J. F. 2019. A single-objective EPR based model for creep index of soft clays considering L2 regularization. Engineering Geology **248**: 242-255.

Leroueil, S., Bouclin, G., Tavenas, F., Bergeron, L., and Rochelle, P. L. 1990. Permeability anisotropy of natural clays as a function of strain. Canadian Geotechnical Journal **27(5)**: 568-579.

Li, P. L., Yin, Z. Y., Song, D. B., Yin, J. H., and Pan, Y. 2024. Axisymmetric finite strain consolidation model for soft soil consolidation with vertical drains under combined loading considering creep and non-Darcy flow. Geotextiles and Geomembranes **52(3)**: 241-259.

Lo, S. R., Mak, J., Gnanendran, C. T., Zhang, R., and Manivannan, G. 2008. Long-term performance of a wide embankment on soft clay improved with prefabricated vertical drains. Canadian Geotechnical Journal **45(8)**: 1073-1091.

Miyakoshi, K., Takeya, K., Otsuki, Y., Nozue, Y., Kosaka, H., Kumagai, M., Oowada, T., and Yamashita, T. 2007. The application of the vacuum compaction drain method to prolong the life of an offshore disposal field. In Nippon Koei Technical Forum **16**: 9-19.

Nagaraj, T. S., and Srinivasa Murthy, B. R. 1986. A critical reappraisal of compression index equations. Géotechnique **36(1)**: 27-32.

Nguyen, B. P., Do, T. H., and Kim, Y. T. 2020. Large-strain analysis of vertical drain-improved soft deposit consolidation considering smear zone, well resistance, and creep effects. Computers and Geotechnics **123**: 103602.

Ni, J., and Geng, X. Y. 2022. Radial consolidation of prefabricated vertical drain-reinforced soft clays under cyclic loading. Transportation Geotechnics **37**: 100840.

Nishimura, S. I., Shimada, K., and Fujii, H. 2002. Consolidation inverse analysis considering spatial variability and non-linearity of soil parameters. Soils and Foundations **42(3)**: 45-61.

Phoon, K. K., and Ching, J. 2012. Beyond coefficient of variation for statistical characterization of geotechnical parameters. Keynote lecture of Geotechnical and Geophysical Site Characterization **4**: 113-130.

Phoon, K. K., and Kulhawy, F. H. 1999. Characterization of geotechnical variability. Canadian Geotechnical Journal **36(4)**: 612-624.

Potts, D. M., and Ganendra, D. 1991. Discussion on “Finite element analysis of the collapse of reinforced embankment on soft ground by Hird C. C., Pyrah I.C., Russel D.”. Géotechnique **41**: 627-630.

Pu, H., Yang, P., Lu, M., Zhou, Y., and Chen, J. N. 2020. Piecewise-linear large-strain model for radial consolidation with non-Darcian flow and general constitutive relationships. Computers and Geotechnics **118**: 103327.

Shi, C., and Wang, Y. 2023. Data-driven spatio-temporal analysis of consolidation for rapid reclamation. Géotechnique **74(7)**: 676-696.

Shimobe, S., and Spagnoli, G. 2022. A general overview on the correlation of compression index of clays with some geotechnical index properties. Geotechnical and Geological Engineering **40(1)**: 311-324.

Song, D. B., Lou, K., Chen, W. B., Wu, P. C., and Yin, J. H. 2024. Finite strain elastic visco-plastic consolidation model for layered soils with vertical drain considering self-weight loading and nonlinear creep. Computers and Geotechnics **169**: 106180.

Song, D. B., Lou, K., Yin, J. H., Fox, P. J., and Chen, W. B. 2023a. A Finite Strain Elastic-Viscoplastic Consolidation Model for Layered Soft Soils Considering Self-Weight and Nonlinear Creep. Journal of Geotechnical and Geoenvironmental Engineering **149(12)**: 04023121.

Song, D. B., Yin, Z. Y., Li, P. L., and Yin, J. H. 2023b. One-dimensional elastic viscoplastic finite strain consolidation model for soft clay with uncertainty. Acta Geotechnica **18(9)**: 4671-4686.

Spagnoli, G., Sridharan, A., Oreste, P., Bellato, D., and Di Matteo, L. 2018. Statistical variability of the correlation plasticity index versus liquid limit for smectite and kaolinite. Applied Clay Science **156**: 152-159.

Spross, J., and Larsson, S. 2021. Probabilistic observational method for design of surcharges on vertical drains. Géotechnique **71(3)**: 226-238.

Sridharan, A., and Nagaraj, H. B. 2000. Compressibility behaviour of remoulded, fine-grained soils and correlation with index properties. Canadian Geotechnical Journal **37(3)**: 712-722.

Tang, M., and Shang, J. Q. 2000. Vacuum preloading consolidation of Yaoqiang Airport runway. Géotechnique **50(6)**: 613-623.

Terzaghi, K. 1943. Theoretical soil mechanics. Wiley, New York.

Wroth, C. P., and Wood, D. M. 1978. The correlation of index properties with some basic engineering properties of soils. Canadian Geotechnical Journal **15(2)**: 137-145.

Yin, J. H. 2015. Fundamental issues of elastic viscoplastic modeling of the time-dependent stress–strain behavior of geomaterials. International Journal of Geomechanics **15(5)**: A4015002.

Yin, J. H., and Graham, J. 1989. Viscous–elastic–plastic modelling of one-dimensional time-dependent behaviour of clays. Canadian Geotechnical Journal **26(2)**: 199-209.

Yin, J. H., and Graham, J. 1994. Equivalent times and one-dimensional elastic viscoplastic modelling of time-dependent stress–strain behaviour of clays. Canadian Geotechnical Journal **31(1)**: 42-52.

Yin, J. H., Chen, W. B., Wu, P. C., Leung, A. Y., Yin, Z. Y., Cheung, C. K., and Wong, A. H. 2024. Field study of a sustainable land reclamation approach using dredged marine sediment improved by horizontal drains under vacuum preloading. Journal of Geotechnical and Geoenvironmental Engineering **150(11)**: 04024114.

Yozzo, D. J., Wilber, P., and Will, R. J. 2004. Beneficial use of dredged material for habitat creation, enhancement, and restoration in New York–New Jersey Harbor. Journal of Environmental Management **73(1)**: 39-52.

Zhu, H., and Zhang, L. M. 2013. Characterizing geotechnical anisotropic spatial variations using random field theory. Canadian Geotechnical Journal **50(7)**: 723-734.

Zhu, W., Yan, J., and Yu, G. 2018. Vacuum preloading method for land reclamation using hydraulic filled slurry from the sea: a case study in coastal China. Ocean Engineering **152**: 286-299.